

# Mossy fiber sprouting in pilocarpine-induced status epilepticus rat hippocampus: A correlative study of diffusion spectrum imaging and histology

Li-Wei Kuo,<sup>a,1</sup> Chun-Yao Lee,<sup>b,1</sup> Jyh-Horng Chen,<sup>a</sup> Van Jay Wedeen,<sup>f</sup> Chih-Chuan Chen,<sup>d</sup> Horng-Huei Liou,<sup>b,d,\*</sup> and Wen-Yih Isaac Tseng<sup>c,e,\*</sup>

<sup>a</sup>Interdisciplinary MRI/MRS Lab, Department of Electrical Engineering, National Taiwan University, Taipei, Taiwan

<sup>b</sup>Department of Pharmacology, National Taiwan University College of Medicine, Taipei, Taiwan

<sup>c</sup>Center for Optoelectronic Biomedicine, National Taiwan University College of Medicine, Taipei, Taiwan

<sup>d</sup>Department of Neurology, National Taiwan University Hospital, Taipei, Taiwan

<sup>e</sup>Department of Medical Imaging, National Taiwan University Hospital, Taipei, Taiwan

<sup>f</sup>Department of Radiology, MGH Martinos Center for Biomedical Imaging, Harvard Medical School, Charlestown, MA, USA

Received 31 August 2007; revised 24 February 2008; accepted 10 March 2008

Available online 20 March 2008

Mossy fiber sprouting (MFS) is the main characteristic of temporal lobe epilepsy (TLE), which is highly correlated with the frequencies of recurrent seizures as well as degrees of severity of TLE. A recent MRI technique, referred to as diffusion spectrum imaging (DSI), can resolve crossing fibers and investigate the intravoxel heterogeneity of water molecular diffusion. Being able to achieve higher accuracy in depicting the complex fiber architecture, DSI may help improve localization of the seizure-induced epileptic foci. In this study, two indices of DSI, which represented the mean diffusivity (MSL) and diffusion anisotropy (DA), were proposed. A correlative study between diffusion characteristics and the severity of MFS was investigated in the pilocarpine-induced status epilepticus (SE) rat model. Nine SE rats and five control rats were studied with MRI and histological Timm's staining. For MSL, no significant correlation was found in the dentate gyrus (DG),  $r=-0.36$ ;  $p=0.2017$ , and positive correlation was found in cornu ammonis (CA3),  $r=0.62$ ;  $p=0.0174$ . The correlation between DA and Timm's score showed positive correlation in DG,  $r=0.71$ ;  $p=0.0047$ , and negative correlation in CA3,  $r=-0.63$ ;  $p=0.0151$ . Our results were compatible with the previous reports on fiber architecture alterations in DG and CA3 subregions. In conclusion, the histological correspondence of DSI indices was demonstrated. With DSI indices, longitudinal follow-up of hippocampal fiber architecture can be

achieved to elucidate the pathophysiology of TLE, which might be helpful in disease localization.

© 2008 Elsevier Inc. All rights reserved.

**Keywords:** Temporal lobe epilepsy; Hippocampus; Mossy fiber sprouting; Diffusion MRI; Diffusion spectrum imaging; Anisotropy; Diffusivity

## Introduction

Temporal lobe epilepsy (TLE) is a common type of focal (localization-related) epilepsy, which is difficult to control with medication (Chang and Lowenstein, 2003). Temporal resection is the most effective treatment for TLE and can provide a better outcome after therapy. Therefore, accurate localization of the epileptic foci is necessary for presurgical planning. To localize the epileptic foci, electroencephalography (EEG) is the most common non-invasive procedure (Duncan, 2007; Duncan et al., 2006). Although EEG has high temporal resolution, its spatial resolution is too low for accurate localization. Conventional magnetic resonance imaging (MRI) and magnetic resonance spectroscopy (MRS) are well-established tools for clinical neuroimaging and have both the sensitivity and specificity for many neurological diseases (Duc et al., 1998; Duncan, 2002). However, successful rates to detect the epileptic foci by conventional MR methods varied and routine evaluation protocols have not been completely established yet. In addition to conventional MR methods, various modalities, such as positron emission tomography (PET) and single photon emission computed tomography (SPECT), were used to

\* Corresponding authors. W.-Y.I. Tseng is to be contacted at Center for Optoelectronic Biomedicine, National Taiwan University College of Medicine, No. 1, Sec 1, Jen-Ai Rd., Taipei, Taiwan 100. Fax: +886 2 2392 6922. H.-H. Liou, Department of Pharmacology and Neurology, National Taiwan University College of Medicine, Room 1141, No. 1, Sec 1, Jen-Ai Rd., Taipei, Taiwan 100. Fax: +886 2 2391 5297.

E-mail addresses: [hhliou@ha.mc.ntu.edu.tw](mailto:hhliou@ha.mc.ntu.edu.tw) (H.-H. Liou), [wytseng@ntu.edu.tw](mailto:wytseng@ntu.edu.tw) (W.-Y.I. Tseng).

<sup>1</sup> These authors contributed equally.

Available online on ScienceDirect ([www.sciencedirect.com](http://www.sciencedirect.com)).

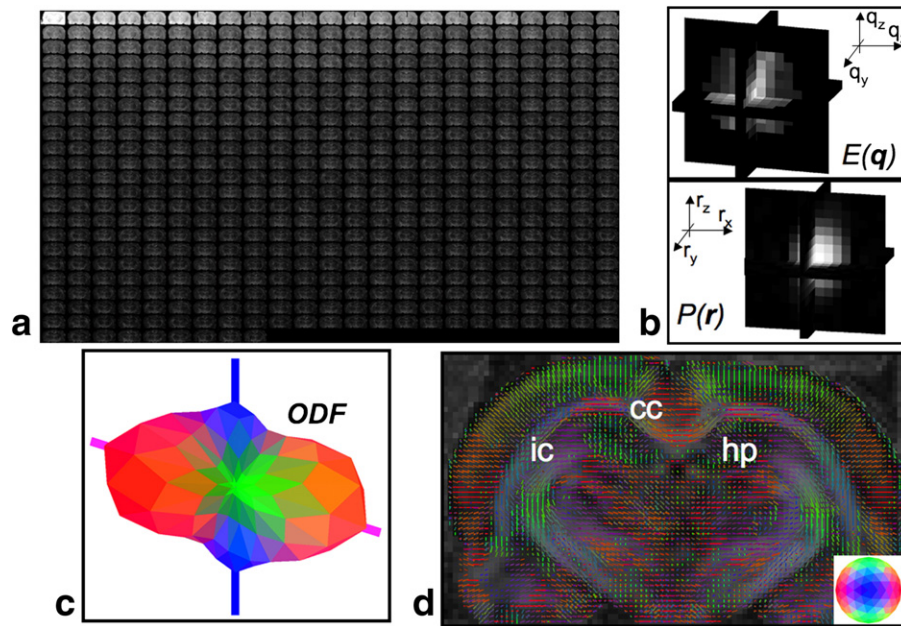


Fig. 1. The procedures for DSI reconstruction. (a) Step 1: 515 diffusion-weighted images were acquired from low  $b$ -value (upper left corner) to maximum  $b$ -value (lower right corner). (b) Step 2: 3D Fourier transform of  $E(\mathbf{q})$  was performed in the  $q$ -space to obtain  $P(r)$  in the PDF space for each voxel. (c) Step 3: second moments of  $P(r)$  along radial directions was computed to obtain ODF. The orientational local maxima are indicated by RGB color-coded fibers. (d) Step 4: a diffusion anisotropy map is overlaid with the color-coded DSI fiber map. (cc: corpus callosum; ic: internal capsule; hp: hippocampus).

study the pathophysiology of epilepsy (Duncan, 2002; Kurian et al., 2007). However, these techniques cannot promise specificity and are difficult to be performed routinely.

The hippocampal formation, the major part of the temporal lobe, controls excitability in the neuronal circuitry and is responsive to an epileptic attack. Mossy fiber sprouting (MFS) is the main characteristic of TLE (Chang and Lowenstein, 2003). Mossy fibers are the axons of granule cells in dentate gyrus (DG) which target to pyramidal cells in cornu ammonis (CA3) region. After epileptic injury, mossy fibers lose their targets due to massive neuronal death in CA3 and hilus area, and form incorrect synaptic connections on the somatic and dendritic sites of granule cells, causing abnormal neuronal circuits and hyperexcitability (Scharfman et al., 2000; Williams et al., 2002). MFS was demonstrated to highly correlate with the frequencies of recurrent seizures as well as degrees of severity of TLE; it was considered an important index to evaluate the severity of TLE in chronic epileptic animal models (Nadler, 2003; Sutula, 2002). Both the granule cell axons and the pyramidal cell axons sprout new collaterals in response to brain injuries. Granule cell axons sprout into the inner molecular layer and hilus, as well as stratum oriens in CA3 (Scharfman, 2007). Pyramidal cell sprouting is believed to play a role in the back-projection circuit in CA3 after brain injury (Scharfman, 2007). However, the underlying mechanism of axonal sprouting in DG and CA3 is not well established.

To conduct animal models of TLE, kainic acid or pilocarpine is injected to cause brain lesions and induce abnormal axonal growths, and the MFS was evaluated by the Timm's staining. The Timm's staining is a sulphide silver method, which is a very sensitive technique for demonstrating the localization of metal and makes the water insoluble metals in tissues visualized (Danscher, 1981). The nerve terminal of mossy fiber contains large amount of Zn ion (Claiborne et al., 1989). After treatment with silver containing developer, the Zn ion in the nerve terminal of mossy

fiber can be captured by the silver and form a dark granules deposition (Zn–S–Ag complex). In an electrophysiological study, Franck et al. reported that there was a correlation between tissue samples with significant Timm's score positivity in the inner molecular layer and slice propensity for bursting when challenged with bicuculline (a proconvulsant) from individuals with intractable temporal lobe seizures (Franck et al., 1995). In addition, in surgically excised DG from epileptic patients underwent lobectomy for refractory partial complex epilepsy, intense Timm's granules are observed in the supragranular region and inner molecular layer, suggesting that MFS may play a role in human epilepsy (Sutula et al., 1989).

The DG plays a critical role in regulating the propagation of seizure activities in hippocampal circuits. In addition, the DG acts as a frequency-dependent filter for paroxysmal activity spreading from the entorhinal cortex and is resistant in response to epileptic injury (Stringer et al., 1989). Significant MFS is observed and considered to recruit reentry excitability in DG to induce spontaneous recurrent seizures. On the other side, CA3 plays a role in integrating

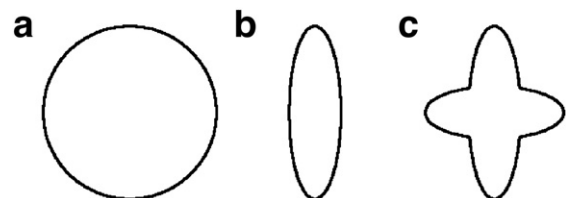


Fig. 2. Illustration of three different shapes of 2D diffusion ODF and their corresponding DA values, (a) isotropic region with  $DA=0$ , (b) single-fiber region with  $DA=0.228$ , and (c) crossing-fiber region with  $DA=0.167$ . For case (c), the ratio of maximum ODF lengths of these two fibers is 5:4. Note that the DA value of the single-fiber region is the highest and that of the crossing-fiber region is relatively lower.

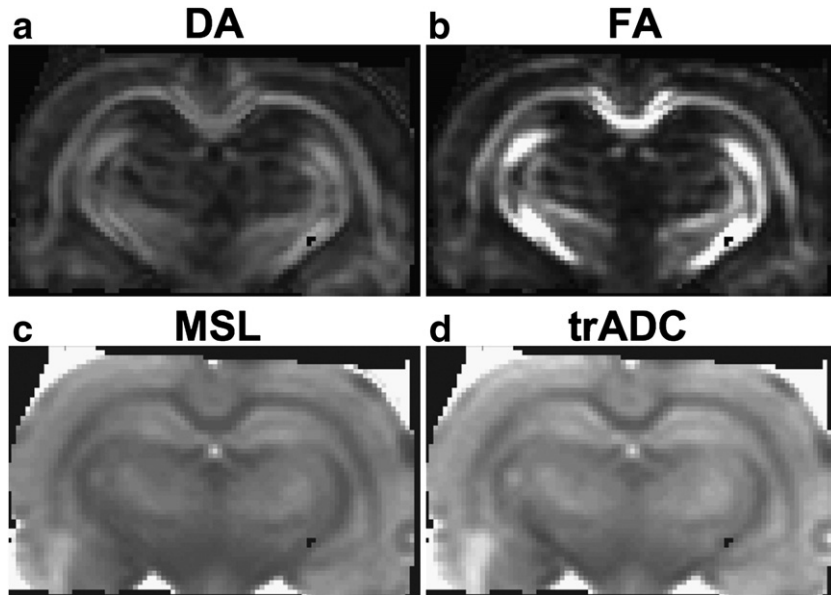


Fig. 3. Diffusion index mapping of a rat brain. Note that image contrast of (a) DSI DA is similar to that of (b) DTI FA, and the contrast of (c) DSI MSL similar to (d) DTI trADC.

the information in the hippocampus. The CA3 pyramidal cells not only receive axonal projection from DG and transmit the signal to CA1, their axons also back-project to DG to regulate its excitability and project to the contralateral part to exchange the information from both sides of hippocampus (Scharfman, 2007). Relatively, CA3 is a vulnerable brain area. Large amount of neuronal loss and axonal sprouting is found in CA3 after epileptic injury (Liu et al., 1999). Dysfunction of CA3 may contribute to abnormality of neuronal circuit inside hippocampus and cause exacerbations of epilepsy. Although the evaluation of Timm's score in DG and CA3 is made according to the condensation of granule deposition in inner molecular layer and stratum oriens, the underlying mechanism of sprouting in these two areas might be disparate. In the current study, therefore, we chose DG and CA3 to study the alteration of axonal fiber architecture in response to epileptic injury by means of the change of diffusion characteristic.

Recently, diffusion tensor imaging (DTI) has become widely used to map fiber orientations and provide quantitative index mapping of the mean diffusivity and anisotropy within each voxel (Basser, 1995). Using scalar diffusion MRI or DTI to study epileptogenic hippocampus has been performed in animal models and human (Fabene et al., 2003; Kimiwada et al., 2006; Rugg-Gunn et al., 2001; Salmenpera et al., 2006; Thivard et al., 2005; van Eijsden et al., 2004). Compared to the normal hippocampus, there is a significant difference in mean diffusivity or fractional anisotropy. Typically in the epileptogenic hippocampus, mean diffusivity increases and anisotropy decreases because of cell loss and fiber sprouting. However, no correlation between these diffusion indices and the histological results was reported. As reviewed by Obenaus and Jacobs, the use of diffusion MRI techniques may provide some information to improve the diagnosis of epilepsy but has not been established as an independent method for diagnosis (Obenaus and Jacobs, 2007). Investigated by another MRI technique, referred to as manganese-enhanced MRI (MEMRI), Nairismagi et al. found significant correlation between

Mn<sup>2+</sup>-enhanced pixel numbers and Timm's score in two hippocampal subregions, DG and CA3 (Nairismagi et al., 2006). Their results indicated that there exists hippocampal axonal plasticity with its severity proportional to Timm's score. Application of diffusion MRI method to depicting structural alteration of hippocampal fiber architecture in correlation with Timm's score, however, is still lacking.

Diffusion spectrum imaging (DSI) was shown to resolve crossing fibers and investigate the heterogeneity of water molecular diffusion within a voxel (Gilbert et al., 2006a,b; Wedeen et al., 2005). DSI is designed to depict complex fiber archi-

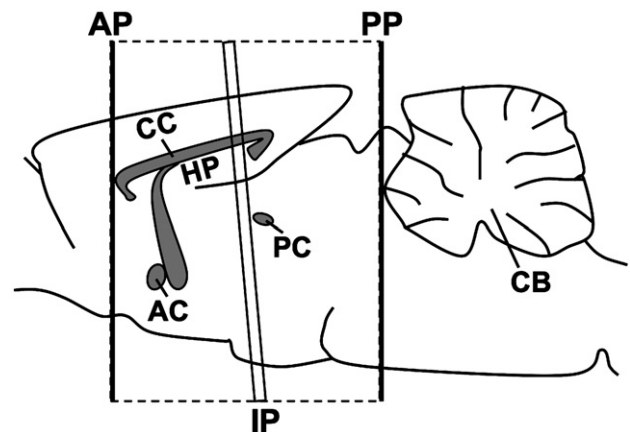


Fig. 4. Planes of dissection and MR imaging of rat hippocampus. Schematic drawing of the midsagittal section of the rat brain (CC: corpus callosum; HP: hippocampus; AC: anterior commissure; PC: posterior commissure; CB: cerebellum) is illustrated. A segment of rat brain was obtained by coronal dissection at the anterior plane (AP) and posterior plane (PP). The dissected specimen was scanned by MR with the imaging plane (IP) perpendicular to the cortical surface of the brain.



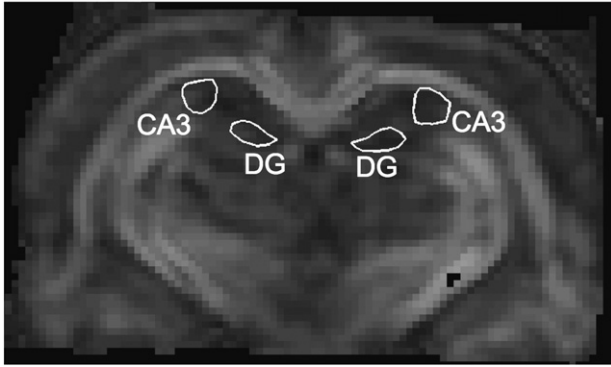


Fig. 6. Illustration of ROIs in DG and CA3. ROIs were selected in DG and CA3 on DA map bilaterally, and identical ROIs were used in both DA and MSL for statistical comparison and correlation study.

texture within each voxel, and may be sensitive to fiber architecture alterations in the seizure-induced epileptic foci (Lin et al., 2003b; Tseng et al., 2002). Therefore, in this paper we aimed to investigate the validity of DSI on an epilepsy rat model. By correlating with histology, we attempted to establish effective diffusion indices that can reflect the histological alterations in the hippocampus.

Two specific DSI indices, namely, mean squared length (MSL) and diffusion anisotropy (DA), were derived to represent the mean diffusivity and diffusion anisotropy, respectively. MSL is a quantitative metric to measure the average translational distance of water molecules under diffusion, which resembles the mean diffusivity or trace ADC of the diffusion tensor. To quantify the shape of the diffusion probability, DA measures the variability of the translational distance in all the radial directions, which resembles the fractional anisotropy (FA) of the diffusion tensor. These two DSI indices were proposed to relate to MFS in the pilocarpine-induced status epilepticus (SE) rat model. Two specific regions of the hippocampus, DG and CA3, were investigated to gain more insight into the effects of epilepsy on fiber architecture in different subregions of the hippocampus. For comparison, we derived DTI indices from the same DSI dataset and performed correlation with histology.

## Theory

### DSI reconstruction

Reconstruction of DSI was based on the Fourier relationship of the attenuated echo signal in q-space  $E(\mathbf{q})$  and the average diffusion propagator of the water molecular diffusion  $P_s(\mathbf{R})$

$$E(\mathbf{q}) = \int P_s(\mathbf{R}, \Delta) \exp(i2\pi\mathbf{q}\mathbf{R}) d\mathbf{R}, \quad (1)$$

where  $\mathbf{R}$  is the relative displacement of water molecular diffusion during the diffusion time  $\Delta$  (Callaghan, 1991). Based on this calculation, applying 3-dimensional (3D) Fourier transform to the echo signal over the q-space would lead us to obtain the 3D

probability density function (PDF) and then map the fiber orientations (Lin et al., 2003b; Wedeen et al., 2005). The transformation from q-space signal to PDF values was performed voxel-by-voxel. To visualize the PDF, the second moment of PDF was integrated along each radial direction to acquire the orientation distribution function (ODF)  $\Psi(\mathbf{u})$ .

$$\Psi(\mathbf{u}) = \int_{r_{\min}}^{r_{\max}} P(r\mathbf{u}) r^2 dr. \quad (2)$$

In this study, ODF within each voxel was reconstructed by interpolating along 162 radial directions, which was calculated from the vertices of a regular and triangular mesh of the unit sphere surface. By comparing the length of each vector  $\Psi(\mathbf{u})$  with the lengths of its neighboring vectors, the orientational local maxima can be obtained to represent intravoxel fiber orientations. The complete procedures to reconstruct DSI and mapping of local maxima are shown in Fig. 1.

### DSI index derivation

Diffusion PDF derived from DSI data was used to quantify the mean diffusivity and diffusion anisotropy within each voxel, which were used to depict the intravoxel diffusion quantitatively. To describe the mean diffusivity, mean squared length (MSL) of water molecular displacement was quantified as the second moment of the normalized PDF over the 3D space, where the probability values were normalized by the probability at zero displacement within each voxel. By this definition, MSL was high in the non-restrictive region and low in the restrictive region. MSL can be formulated as the following,

$$MSL = \int_{\text{PDF}} r^2 P(r, \Delta) dr = \langle r^2 \rangle, \quad (3)$$

where integration was performed over the whole PDF space.

Diffusion anisotropy is a metric to quantify the shape of the probability of water molecular diffusion, which further implies the fiber structures of the tissues. To derive diffusion anisotropy from DSI (DA), the standard deviation (*std*) of the normalized ODF was computed, indicating the anisotropy within each voxel,

$$DA = \text{std}(\Psi), \quad (4)$$

where  $\Psi$  represents the vector lengths of all ODFs within each voxel. All ODFs were normalized by the maximum ODF length within each voxel. As illustrated in Fig. 2, DA is approximately zero in regions with isotropic diffusion such as cerebrospinal fluid because there is little variability of ODFs in all directions (Fig. 2a). In contrast, DA is the highest in white matter fibers with single coherent direction where diffusion is highly anisotropic (Fig. 2b). In the case of crossing fibers the DA is intermediate, and its value varies with the crossing angle between individual fibers, as well as the relative volumes and difference in DA (Fig. 2c).

Fig. 5. Examples of the histological stains in DG (left column) and CA3 (right column), corresponding to Timm's scores ranged from 0 to 5. The severity of MFS increased as Timm's score became higher. The arrows indicated deposition of granules (evidence of axonal sprouting) under Timm's staining. The slice thickness of staining was 30  $\mu\text{m}$ .

### DTI reconstruction from DSI dataset

Since a large proportion of DSI data is acquired using substantially large  $b$ -values by which signal intensity is heavily attenuated. DTI reconstructed from the whole DSI dataset would suffer from low signal-to-noise ratio (SNR). To obtain the optimum sub-sampled dataset for DTI reconstruction, the relationship between SNR and the number of sub-sampled DSI dataset was investigated. Note that the maximum diffusion sensitivity (maximum  $b$ -value,  $b_{\max}$ ) of our DSI dataset was 27000 s/mm<sup>2</sup> and sampled on the grid points with the radius  $|q| \leq 5$  units in the  $q$ -space, so the  $b$ -value at any grid point ( $q_x, q_y, q_z$ ) in the  $q$ -space can be computed by  $27000 \times (q_x^2 + q_y^2 + q_z^2) / 5^2$  according to the proportionality between  $|q|^2$  and the  $b$ -value. The SNR was defined as  $\sqrt{N} \times e^{-b_{\text{avg}} D}$ , where  $N$  is the number of sub-sampled dataset,  $b_{\text{avg}}$  is the average  $b$ -value and  $D$  is the diffusion coefficient, approximately  $2 \times 10^{-4}$  mm<sup>2</sup>/s in ex vivo brains (Shepherd et al., 2006). Based on our DSI data, we found that the optimum dataset for DTI reconstruction was the sub-sampled dataset with  $N=81$  ( $|q| \leq 2.45$  units and  $b_{\text{avg}}=4560$  s/mm<sup>2</sup>). Bito et al. proposed that the optimal diffusion weighting for diffusivity measurements could be estimated by  $b=1.11 / \text{ADC}$  (Bito et al., 1995). Jones et al. later showed that if transverse relaxation was taken into consideration, the estimated optimal  $b$  factor was 30% less than Bito's, i.e.  $b=0.78/\text{ADC}$  (Jones et al., 1999). Based on the above equations, the optimal  $b$ -value ranges from 3850 to 5500 s/mm<sup>2</sup> provided  $\text{ADC}=2 \times 10^{-4}$  mm<sup>2</sup>/s in the brain tissue. The estimated  $b$ -value is very close to the average  $b$ -value of 4560 s/mm<sup>2</sup> in our optimum sub-sampled dataset for DTI reconstruction.

### Index mapping of DSI vs. DTI

We reconstructed DTI using the optimum sub-sampled dataset as described above. The DTI indices, FA and trADC, were computed from the diffusion tensor according to the standard definition (Basser,

1995). As shown in Fig. 3, similar contrast can be appreciated between DSI DA and DTI FA mapping, and between DSI MSL and DTI trADC mapping.

### Materials and methods

#### Pilocarpine-induced SE rat model and brain tissue preparation

A total of fourteen rats, five for control group and nine for SE group, were used in this study. The Institutional Animal Care and Use Committee at National Taiwan University approved all the animal procedures. Male Wistar rats (150–180 g, age 1 month) were injected with pilocarpine (300–380 mg/kg, intraperitoneally, i.p.) to induce SE. The behavioral seizure was evaluated according to Racine's score: stage 1, facial and body tremors; stage 2, myoclonic jerk of the whole body; stage 3, clonic convulsions of the whole body; stage 4, clonic-convulsions with flexion of hind limbs; stage 5, clonic-convulsions with extension of hind limbs (Racine, 1972). SE was defined as continuous convulsions with a score of 4 to 5 for at least 1 h and terminated by pentobarbital (25–30 mg/kg, i.p.). The MFS in the pilocarpine-induced SE rat model is known to be a tissue damage that could keep life long. As reported by Mello et al., Timm's score in DG was highly correlated with age (Mello et al., 1993). MFS in DG begins to appear early (4 days) after SE induction and reaches a plateau by approximately 100 days. Furthermore, the MFS was found to persist for at least 374 days after injection (Mello et al., 1993). In our study, the animals were kept for 1 or 3 months after SE (four for 1 month and five for 3 months) and were sacrificed for MRI experiment and histological observation during the progression of MFS. After deep anesthesia with pentobarbital (80 mg/kg, i.p.), rats were perfused transcardially with 200 ml of sodium sulfide perfusion medium (2.925 g Na<sub>2</sub>S, 2.975 g NaH<sub>2</sub>PO<sub>4</sub>; H<sub>2</sub>O in 500 ml distilled H<sub>2</sub>O) followed by 200 ml 4% paraformaldehyde. Due to the limitation of the sample size placed within the volume transmit/receive RF coil of diameter of 3.5 cm, rat

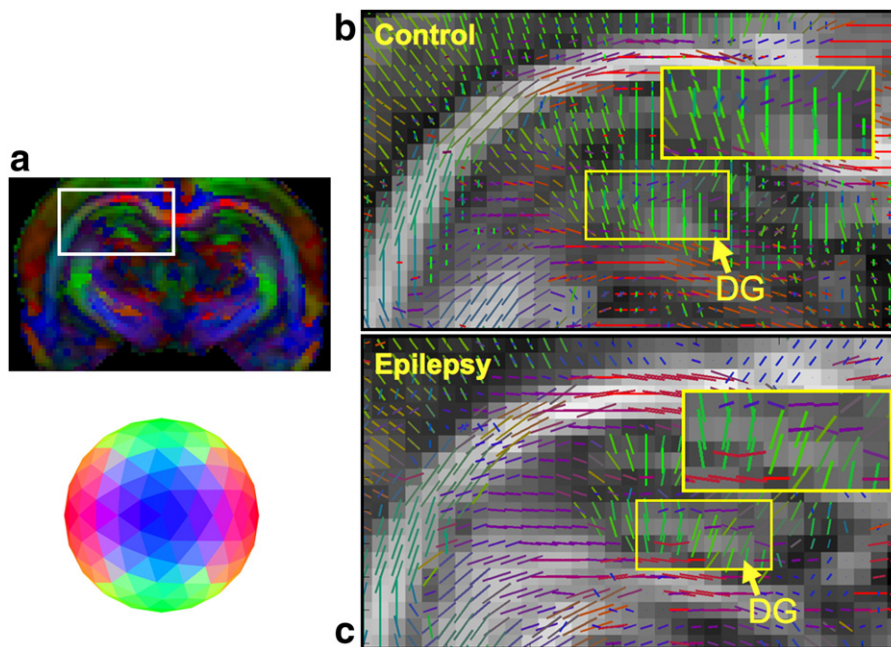


Fig. 7. (a) A color-coded orientation map of a rat brain. Zoom-in views of right hippocampus are indicated by the white squares. The yellow arrows indicate the regions of DG, which are zoomed in the yellow squares. Diffusion anisotropy maps are overlaid with a DSI fiber map in (b) a control rat and (c) an SE rat. The fibers were RGB color-coded based on their orientations as illustrated in the color sphere.

brains were dissected from the cranium and fixed in a glass vial filled with 4% paraformaldehyde solution for overnight post-fixation. After fixation, the brains were transferred from paraformaldehyde to phosphate buffer solution (PBS) for at least 1 week before MRI scanning. This allowed brains to immerse long enough to achieve equilibrium in PBS solution. To provide clear geometrical markers for localizing histological sections to the MRI slice, a segment of rat brain was dissected with two parallel cut surfaces, one in anterior plane (AP) and another in posterior plane (PP) (Fig. 4). During localization of the MRI slice, the distance between AP (at Bregma +1.2 mm) and the imaging plane (IP) (at Bregma -3.8 mm) was recorded (Paxinos and Watson, 1996). The distance was then used for determining the histological staining sections those were located within the thickness of the MRI slice. In this way, we restricted the angular difference between the MR imaging plane (IP) and histological sectioning planes (AP) to less than 10°. During the MRI experiment, the dissected brain was placed in a plastic box (2.5 × 1.5 × 1.5 cm<sup>3</sup>) with PBS, and inserted into the center of the volume RF coil.

#### MRI experiment

MRI experiments were performed on a 3T MRI system (Bruker Biospin, Ettlingen, Germany) in an inserted gradient system, a standard product of Bruker Biospec system and typed with G060. The diameter of the gradient bore is 7 cm with the maximum gradient strength=950 mT/m and a rise time=50 μs (5%~95%). The maximum diffusion gradient strength applied in this study was 90% of 950 mT/m (850 mT/m). During the experiment, the gradient insert was hinged inside the 3T magnet. A fast spin-echo T2-weighted sequence, rapid acquisition with relaxation enhancement (RARE), was performed to localize the desired slice position. Diffusion-weighted images (DWI) of DSI were acquired using pulsed-gradient spin-echo (PGSE) sequence with 515 diffusion-encoding gradients. These encodings corresponded to grid points in 3D q-space. The spatial modulation was  $q = \gamma g \delta / 2\pi$ , where  $\gamma$  is the proton gyromagnetic ratio,  $g$  is the diffusion-encoding gradient and  $\delta$  is the diffusion gradient duration. The imaging parameters were TR/TE=1000/25.7 ms, number of excitation (NEX)=2, and diffusion time/diffusion gradient duration=15/6.3 ms, yielding the  $b_{\max}$  of approximately 27000 s/mm<sup>2</sup>. The resolutions of q-space and probability domains were 0.047 μm<sup>-1</sup> and 4.3 μm, respectively, resulting in the field-of-view (FOV) of 21.5 μm in the spatial domain. The slice thickness was 1 mm and single slice was acquired for each rat. Using imaging FOV of 22 × 11 mm<sup>2</sup> and matrix size of 128 × 64, which was zero-filled from the original matrix size of 64 × 32, we obtained images with in-plane resolution of 172 × 172 μm<sup>2</sup>. The total scan time of each DSI acquisition was approximately 11 h.

#### Timm's staining

Timm's staining was performed to evaluate the severity of MFS right after each MRI experiment to obtain the histological results for correlation analysis. The brains were transferred in a 30% sucrose solution for dehydration until the brains sank to the bottom of the vial. For histology, 30-μm-thick brain tissue was sectioned by a freezing microtome throughout the entire extent of the dissected brain with the sectioning plane being parallel to AP (Fig. 4). These sections were then attached on coated glass slides. Based on the distance between AP and IP for each rat, we determined the histological sections that were located within the thickness of the MRI slice. We stained one in every six sections, amounting to approximately 36 sections for each

rat, and calculated the Timm's scores of these stained sections based on the following procedures. The sections were developed in the dark for 45 min in a solution of 50% Arabic gum (120 ml), 10 ml citric acid (51 g/100 ml H<sub>2</sub>O), 10 ml sodium citrate (47 g/100 ml H<sub>2</sub>O), 3.47 g hydroquinone in 60 ml, and 212.25 mg AgNO<sub>3</sub>. After washing, the slices were dehydrated in graded alcohol, cleared in xylene, and mounted on slides with Permount. There were five scores to calculate the severities of MFS in DG (Cilio et al., 2003): score 0, no granules noted between crest and tips in the supragranular region; score 1, occasional granules in the supragranular region occurring in patchy distribution; score 2, numerous granules in the supragranular region occurring in patchy distribution; score 3, granules in the supragranular region occurring in near-continuous distribution; score 4, highly concentrated band of granules appearing either in continuous or near-continuous distribution; score 5, continuous dense laminar band of granules from the crest to the tip of the dentate. Similarly, there were five scores to calculate the severities of MFS in CA3: score 0, No granules in the stratum pyramidale or stratum oriens along any portion of the CA3 subregion; score 1, occasional granules in the stratum

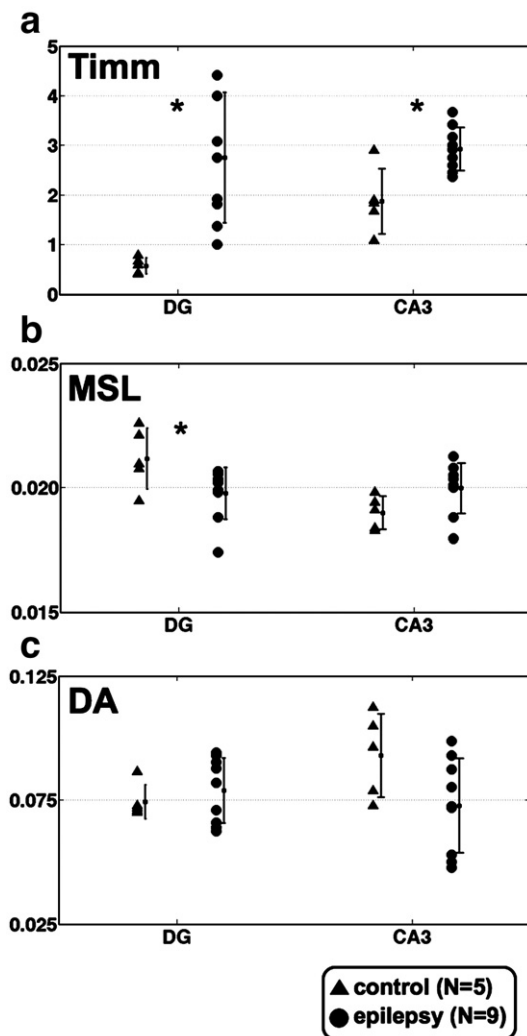


Fig. 8. Comparison between the control ( $N=5$ ) and SE ( $N=9$ ) groups for (a) Timm's score, (b) MSL (a.u.), and (c) DA. The average and standard deviation values of the control and SE groups are indicated by the error bars. (\* $p < 0.05$ ).

pyramidale or stratum oriens occurring in discrete bundles; score 2, occasional to moderate granules in the stratum pyramidale or stratum oriens; score 3, prominent granules in the stratum pyramidale or stratum oriens; score 4, prominent granules in the stratum pyramidale or stratum oriens occurring in near-continuous distribution along the entire CA3 region; score 5, continuous or near-continuous dense laminar band of granules in the stratum pyramidale or stratum oriens along the entire CA3 region. We calculated the Timm's score by each section and averaged all the scores of these stained sections as one rat's Timm's score for DG and CA3 accordingly. The stained sections were analyzed for each rat by one of the authors (CYL) blind to experimental groups and analyzed by using a semiquantitative scale for supragranular layer of the DG and terminal sprouting CA3 pyramidal cell region. Examples of histological stains of DG and CA3 are shown in Fig. 5, revealing different levels of MFS.

#### Statistical analysis

DSI reconstruction and statistical analysis were performed using in-house written program in MATLAB 7.0 (The Mathworks, Natick, MA, USA). To derive DSI indices within specific regions for comparison, regions-of-interest (ROIs) of CA3 and DG were manually selected on DA map by two of the authors (LWK, CYL) (Fig. 6). The values of DA and MSL were derived from the identical position of ROIs. These ROIs were selected bilaterally in the hippocampal regions and the average values were derived to indicate the representative values of all the compared regions. Comparisons of Timm's score, DA and MSL between the control and SE groups were performed using analysis of variance.

Pearson's correlation coefficient ( $r$ ) was derived to investigate the relationship between the DSI indices and Timm's score. The same analysis was also performed on DTI indices.

#### Results

Mapping of hippocampal fiber structure in a control rat and an SE rat are shown in Fig. 7. For both maps, the fiber bundles of the corpus callosum were well organized, indicating satisfactory and comparable data quality. Compared with the control rat, the fibers in DG regions of the SE rat were partially disorganized with slightly decreased regions of crossing fibers.

To test the stability of DSI indices, a circular ROI with a radius of 3 pixels was selected on the right primary somatosensory cortex (S1), located laterally from CA3 of the right hippocampus. The average and standard deviation of DSI indices of all the rats were computed; DA was  $0.065 \pm 0.008$  and MSL (a.u.) was  $0.021 \pm 0.002$ .

In Fig. 8a, the average Timm's scores of the control and SE groups were compared and showed a significant difference between the two groups. In DG, the average Timm's score of the SE rats was  $2.75 \pm 1.24$ , significantly higher than that of the control rats,  $0.57 \pm 0.15$ ;  $p < 0.05$ . Similarly, in CA3, the average Timm's score of the SE rats was  $2.93 \pm 0.41$ , significantly higher than that of the control rats,  $1.87 \pm 0.59$ ;  $p < 0.05$ .

Comparison of MSL between the control and SE groups is shown in Fig. 8b. In DG, the average MSL (a.u.) of the control rats was  $0.0212 \pm 0.0012$ , significantly higher than that of the SE rats,  $0.0198 \pm 0.0010$ ;  $p < 0.05$ . In CA3, no significant difference was

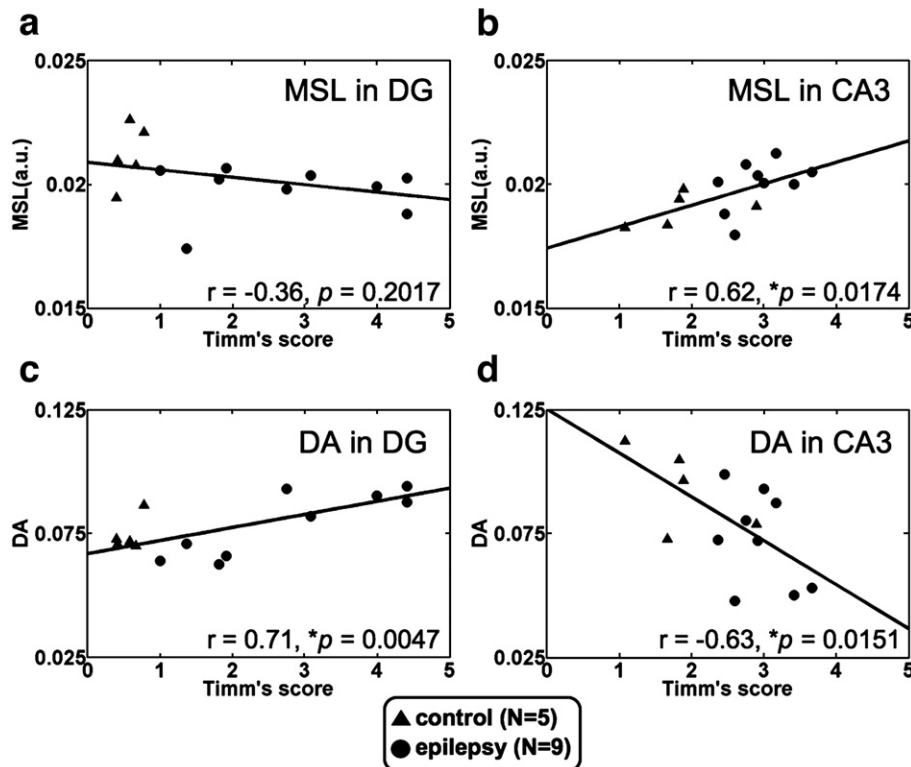


Fig. 9. MSL (a–b) and DA (c–d) were correlated against Timm's score in DG and CA3. (a) No significant correlation (MSL) in DG ( $r = -0.36$ ,  $p = 0.2017$ ). (b) Positive correlation (MSL) in CA3 ( $r = 0.62$ ,  $p = 0.0174$ ). (c) Positive correlation (DA) in DG ( $r = 0.71$ ,  $p = 0.0047$ ). (d) Negative correlation (DA) in CA3 ( $r = -0.63$ ,  $p = 0.0151$ ). ( $*p < 0.05$ ).

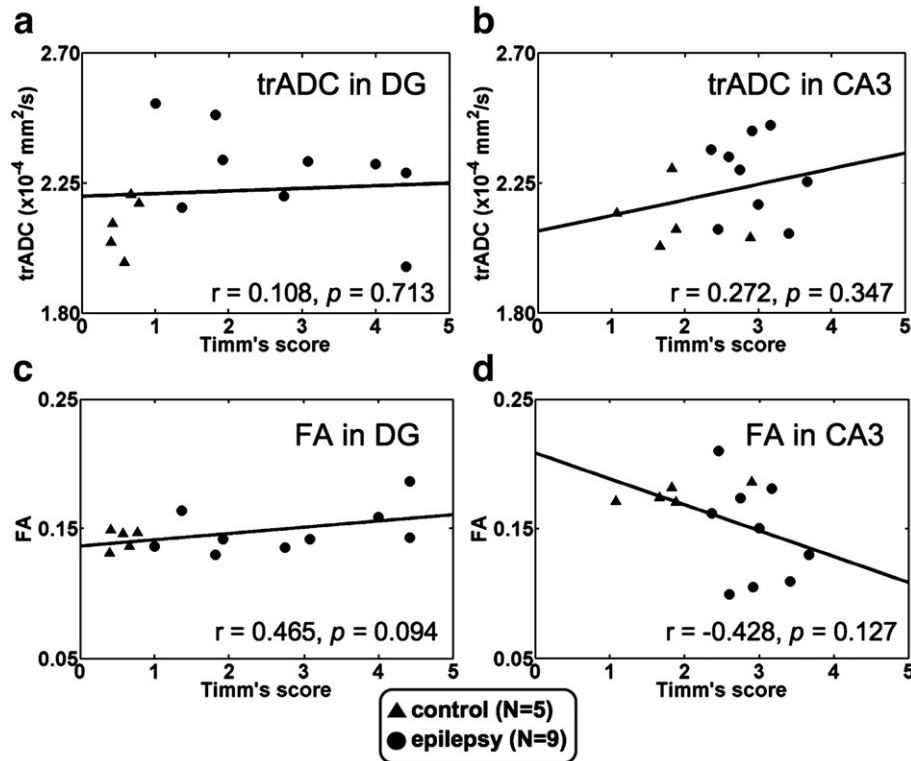


Fig. 10. DTI trADC (a–b) and FA (c–d) were correlated against Timm's score in DG and CA3. No significant correlation was found in the following comparisons, (a) trADC in DG ( $r=0.108$ ,  $p=0.713$ ), (b) trADC in CA3 ( $r=0.272$ ,  $p=0.347$ ), (c) FA in DG ( $r=0.465$ ,  $p=0.094$ ) and (d) FA in CA3 ( $r=-0.428$ ,  $p=0.127$ ).

observed between the control and SE rats,  $0.0190 \pm 0.0007$  vs.  $0.0200 \pm 0.0010$ ;  $p > 0.05$ .

Comparison of DA between the control and SE groups is shown in Fig. 8c. In DG, no significant difference was observed between the control and SE rats,  $0.0743 \pm 0.0068$  vs.  $0.0789 \pm 0.0131$ ;  $p > 0.05$ . Similarly, there was no significant difference in CA3,  $0.0930 \pm 0.0169$  and  $0.0727 \pm 0.0190$ ;  $p > 0.05$ .

The results of correlation between MSL and Timm's score are shown in Figs. 9a and b. No significant correlation was found in DG region,  $r=-0.36$ ;  $p=0.2017$ , and positive correlation was found in CA3,  $r=0.62$ ;  $p=0.0174$ . The correlation between DA and Timm's score showed positive correlation in DG,  $r=0.71$ ;  $p=0.0047$ , and negative correlation in CA3,  $r=-0.63$ ;  $p=0.0151$  (Figs. 9c and d).

The correlation analysis between DTI indices (trADC and FA) and Timm's score within the same ROI location in DG and CA3 was performed on the same rats (five control and nine SE rats). Fig. 10 shows the scatter plots of DTI indices against Timm's score in DG and CA3. For both DTI indices, no significant correlation is found in DG and CA3. For trADC,  $r=0.108$  ( $p=0.713$ ) in DG (Fig. 10a) and  $r=0.272$  ( $p=0.347$ ) in CA3 (Fig. 10b). For FA,  $r=0.465$  ( $p=0.094$ ) in DG (Fig. 10c) and  $r=-0.428$  ( $p=0.127$ ) in CA3 (Fig. 10d).

## Discussion

In this study, we proposed two DSI indices, MSL and DA, representing the mean diffusivity and diffusion anisotropy, respectively, to study their histological correspondence in the hippocampus.

Compared with the control rats, SE rats showed significantly higher Timm's scores in both DG and CA3 subregions, whereas the difference in DA and MSL between the two groups was not significant. When DA and MSL of all rats were correlated against Timm's scores, disparate results of correlation were observed in DG and CA3. In DG, we found positive correlation between DA and Timm's score, and no correlation between MSL and Timm's score. In CA3, we found negative correlation between DA and Timm's score, and positive correlation between MSL and Timm's score.

From the DSI fiber maps (Fig. 7), coherent fibers in the corpus callosum and distinct layered fiber architecture in the hippocampus could be readily observed. Although mild disorientation of hippocampal fiber architecture existed in the SE rat, the changes were too mild to be detected reliably. By analyzing DA and MSL, these DSI indices were demonstrated to indicate the severity of MFS in different subregions of hippocampus. As shown in the results, the stability of DSI indices was ensured by the narrow inter-subject variability of these indices in the primary somatosensory cortex S1.

In this study, we found significant differences in Timm's score between the control and SE rats in both DG and CA3, compatible with the current knowledge that Timm's score reflects the severity of MFS (Cilio et al., 2003). By comparing DSI indices between these two groups, the SE rats had higher values of DA, but statistically insignificant, and lower values of MSL in DG, statistically significant. In CA3, the SE rats showed lower values of DA and higher values of MSL, but both failed to achieve statistical significance. These findings suggest that the change in diffusion indices is subregion-dependent and is modulated not only

by MFS but also by other factors such as cell loss and fiber crossing. Although the results indicated a minimal subregion-dependent difference, the number of rats used in this study was insufficient to achieve the statistical threshold.

In previous diffusion studies on the pilocarpine-induced SE rat model, Fabene et al. studied the rat brain 12 h after the end of pilocarpine-induced SE, and found that the ADC value was increased by 16% in the epileptogenic hippocampus, in which structural disintegration and neuronal injury occurred (Fabene et al., 2003). van Eijsden et al. reported that ADC value of the epileptogenic hippocampus was increased significantly at 3 h after SE but no significant difference was observed at 5 h after SE (van Eijsden et al., 2004). Wall et al. followed 3, 6, 12 and 24 h after SE and found that an ADC rise of 19% was observed in the hippocampus at 24 h after SE (Wall et al., 2000). In our study, a mild tendency of increasing MSL was observed in CA3, which was consistent with those previous studies. However, the difference was not significant, which may be explained by the decline of mean diffusivity in the epileptogenic hippocampus during the chronic stage (Nairismagi et al., 2004). In DG, we found a significant decrease of MSL, which was opposite to those previous studies. This difference may be caused by the method of ROI selection, which we focused on DG and CA3 separately, but most of them used whole hippocampus for analysis. Mean diffusivity may vary in different subregions of hippocampus so that the change we observed in these two MFS-related subregions was not global.

In DG, DA showed positive correlation with Timm's score. Since Timm's score is a semiquantitative representation of the severity of MFS, our results imply that translational motion of water molecules becomes more preferable along fiber direction as the mossy fibers in DG increase. As reported, the mossy fibers in DG are relatively homogeneous within the hippocampus and the DG has been proposed to receive information with more selective needs for hippocampal processing (Scharfman, 2007; Scharfman et al., 2002). Kim et al. reported that the granule cells in DG growing on the stratum granulosum displayed a preference of axon orientation toward the dentate hilus, whereas those misplaced onto CA1 or CA3 stratum pyramidale exhibited no such preference even though they were located adjacent to CA3 stratum lucidum, a normal recipient site of mossy fibers (Kim et al., 2004). Compatible with previous reports (Buckmaster and Dudek, 1997; Cronin and Dudek, 1988), our finding suggests that the increased MFS in DG might accompany with more preferential orientation and higher regularity of fiber structure, resulting in increased DA. Therefore, increased MFS in DG could contribute to the positive correlation between DA and Timm's score. However, owing to the higher regularity of fiber structure, increased diffusivity along fiber direction and decreased diffusivity in cross-fiber direction may lead to a combinatorial effect to the slightly decreased MSL but insignificant.

In CA3, DA showed negative correlation and MSL showed positive correlation with Timm's score. This indicates that the fiber structure in CA3 becomes more heterogeneous as MFS increases. It has been shown that fibers coming from DG and CA1 intersect in CA3, resulting in heterogeneous generation of MFS after SE (Scharfman, 2007). It is also known that there is massive neuronal loss in CA3 and hilus region during MFS (Mello et al., 1993; Siddiqui and Joseph, 2005). Consequently, disorientated fiber sprouting, empty space after neuronal loss, and reorganization of local neuronal circuits make the fiber structure in CA3 more heterogeneous, and simultaneously affect the changes in DA and MSL.

In this study, we did not perform another separate DTI acquisition for each rat, and so cannot perform DSI vs. DTI comparison on a fair basis. As proposed by Jones and Basser, diffusion tensors reconstructed from DSI dataset with predominant high- $b$ -value images (in our case,  $b_{\max}=27000$  s/mm<sup>2</sup> and  $b_{\text{avg}}=16000$  s/mm<sup>2</sup> is subjected to noise errors and unwanted artifacts (Jones and Basser, 2004). Therefore, we estimated a subset of DSI data which was most appropriate for reconstructing the diffusion tensor, and then performed DTI reconstruction using this sub-sampled data set. Our approach, in fact, can be viewed as a low pass filter applied to the whole DSI data to prevent the errors. The DTI results, in terms of the strength of association with MFS, were then compared with the DSI results.

Although the strength of association between DTI indices and Timm's score is not significantly strong in both areas, we can still see a similar tendency of correlation as noted in DSI indices. The results of our DTI analysis do not imply that DTI is less sensitive than DSI in correlating MFS because the data were not acquired optimally for DTI. Although DTI is limited in resolving intravoxel fiber crossing, the limitation could be partly ameliorated by increasing spatial resolution. Therefore, it is of great interest to compare the capability of DTI and DSI in correlating MFS on a fair basis. Under the same scan time, DTI can achieve higher SNR than DSI because the  $b$ -values of DTI are substantially lower than the average  $b$ -values of DSI. If DTI is acquired with SNR similar to DSI, the extra amount of SNR can be traded for higher spatial resolution. This may reduce the partial volume effect and define fiber orientation more accurately (Shepherd et al., 2006). The accuracy of mapping fiber orientation also depends on the number and  $b$ -value of diffusion-encoding gradients and sampling schemes. All of these factors need to be taken into consideration in order to perform a fair comparison between DTI and DSI. Although important and interesting, such comparative study is beyond the scope of our study.

A recent technique, referred to as manganese-enhanced MRI (MEMRI), correlated mossy fiber plasticity with the number of enhanced pixels in DG and CA3 (Nairismagi et al., 2006). Fourteen kainic-acid induced SE rats and five control rats were compared, which were injected with MnCl<sub>2</sub> at 2 weeks after SE. After 3 and 5 days of Mn<sup>2+</sup> injection, MEMRI and correlation study were performed. Significant positive correlation was found between Mn<sup>2+</sup>-enhanced pixel numbers and Timm's score, suggesting that MEMRI can reveal significant structural plasticity. In our results, structural mossy fiber plasticity was revealed by observing the correlation between DSI characteristics and Timm's score. Furthermore, our findings suggested that subregion-dependent change of MFS occurred differently in DG and CA3. In DG, mossy fibers sprouted compactly, whereas the sprouting was heterogeneous in CA3. Thus, these two techniques, DSI and MEMRI, can be further combined to localize and observe the epileptic foci accurately.

The histological correlation of DSI in the epileptogenic hippocampus was successfully demonstrated in this study; however, there are still several difficulties before the procedure can be used for routine clinical diagnosis of epilepsy. First, compared to conventional MRI or DTI, the total scan time of DSI was still too long, which significantly limited its feasibility. Therefore, parallel imaging techniques or reduced encoding schemes have to be applied to improve the temporal limitation of DSI (Chiang et al., 2006; Jaermann et al., 2004; Lin et al., 2003a; Reese et al., 2006). Second, imaging specific subregions of human hippocampus required sufficient spatial resolution beyond what is

found in a typical setting, which may also reduce the signal-to-noise ratio (SNR) significantly (Shepherd et al., 2003). This may be overcome by improved hardware, such as high-strength head gradient, which can achieve sufficient spatial resolution and provide stable  $b_{\max}$  for diffusion encoding, and high-performance RF coil, which can provide sufficient SNR for data acquisition. Third, the artifacts of echo-planar imaging (EPI), such as susceptibility artifact and eddy current, or motion artifact during DSI acquisition, may increase the bias of ROI selection (Le Bihan et al., 2006). To correct the susceptibility and eddy current, novel sequences were proposed (Reese et al., 2003; Shepherd et al., 2003). To reduce motion artifacts, on-line navigating or post-processing methods can be applied (Mori and van Zijl, 1998; Weih et al., 2004). With these technical improvements, it is possible to apply DSI to monitoring epileptogenesis in a clinical setting.

In conclusion, a rat model of pilocarpine-induced TLE was used to test the feasibility of the proposed DSI indices, DA and MSL, to detect MFS in the hippocampus. Disparate correlations between diffusion indices and severity of MFS were observed in DG and CA3. Our results suggest that the change in DSI indices was the result of combinatorial alterations of fiber structure and neuronal loss and is thus, subregion-dependent. DSI indices are potentially useful to monitor the progress of structural abnormality in epileptic patients and might be helpful in localization of epileptic foci.

## Acknowledgments

The work was supported in part by the grants NSC95-2752-M-002-018-PAE, NHRI-EX96-9308ES and NSC95-2323-B-002-005. We are grateful to Dr. Kai-Hsiang Chuang for his helpful comments.

## References

- Basser, P.J., 1995. Inferring microstructural features and the physiological state of tissues from diffusion-weighted images. *NMR Biomed.* 8, 333–344.
- Bito, Y., Hirata, S., Yamamoto, E., 1995. Optimal gradient factors for ADC measurements. *Proc. Int. Soc. Magn. Reson. Med. ISMRM, California*, p. 913.
- Buckmaster, P.S., Dudek, F.E., 1997. Neuron loss, granule cell axon reorganization, and functional changes in the dentate gyrus of epileptic kainate-treated rats. *J. Comp. Neurol.* 385, 385–404.
- Callaghan, P.T., 1991. Principles of nuclear magnetic resonance microscopy. Clarendon Press, Oxford.
- Chang, B.S., Lowenstein, D.H., 2003. *Epilepsy*. *N. Engl. J. Med.* 349, 1257–1266.
- Chiang, W.Y., Wedeen, V.J., Kuo, L.W., Peng, M.H., Tseng, W.Y., 2006. Diffusion spectrum imaging using Body-Center-Cubic sampling scheme. *Proc. Int. Soc. Magn. Reson. Med. ISMRM, California*, p. 1041.
- Cilio, M.R., Sogawa, Y., Cha, B.H., Liu, X., Huang, L.T., Holmes, G.L., 2003. Long-term effects of status epilepticus in the immature brain are specific for age and model. *Epilepsia* 44, 518–528.
- Claiborne, B.J., Rea, M.A., Terrian, D.M., 1989. Detection of zinc in isolated nerve terminals using a modified Timm's sulfide-silver method. *J. Neurosci. Methods* 30, 17–22.
- Cronin, J., Dudek, F.E., 1988. Chronic seizures and collateral sprouting of dentate mossy fibers after kainic acid treatment in rats. *Brain Res.* 474, 181–184.
- Dansch, G., 1981. Histochemical demonstration of heavy metals. A revised version of the sulphide silver method suitable for both light and electron microscopy. *Histochemistry* 71, 1–16.
- Duc, C.O., Trabesinger, A.H., Weber, O.M., Meier, D., Walder, M., Wieser, H.G., Boesiger, P., 1998. Quantitative <sup>1</sup>H MRS in the evaluation of mesial temporal lobe epilepsy in vivo. *Magn. Reson. Imaging* 16, 969–979.
- Duncan, J.S., 2002. Neuroimaging methods to evaluate the etiology and consequences of epilepsy. *Epilepsy Res.* 50, 131–140.
- Duncan, J.S., 2007. Epilepsy surgery. *Clin. Med.* 7, 137–142.
- Duncan, J.S., Sander, J.W., Sisodiya, S.M., Walker, M.C., 2006. Adult epilepsy. *Lancet* 367, 1087–1100.
- Fabene, P.F., Marzola, P., Sbarbati, A., Bentivoglio, M., 2003. Magnetic resonance imaging of changes elicited by status epilepticus in the rat brain: diffusion-weighted and T2-weighted images, regional blood volume maps, and direct correlation with tissue and cell damage. *NeuroImage* 18, 375–389.
- Franck, J.E., Pokorny, J., Kunkel, D.D., Schwartzkroin, P.A., 1995. Physiologic and morphologic characteristics of granule cell circuitry in human epileptic hippocampus. *Epilepsia* 36, 543–558.
- Gilbert, R.J., Magnusson, L.H., Napadow, V.J., Benner, T., Wang, R., Wedeen, V.J., 2006a. Mapping complex myoarchitecture in the bovine tongue with diffusion-spectrum magnetic resonance imaging. *Biophys. J.* 91, 1014–1022.
- Gilbert, R.J., Wedeen, V.J., Magnusson, L.H., Benner, T., Wang, R., Dai, G., Napadow, V.J., Roche, K.K., 2006b. Three-dimensional myoarchitecture of the bovine tongue demonstrated by diffusion spectrum magnetic resonance imaging with tractography. *Anat. Rec., A. Discov. Mol. Cell. Evol. Biol.* 288, 1173–1182.
- Jaermann, T., Crelier, G., Pruessmann, K.P., Golay, X., Netsch, T., van Muiswinkel, A.M., Mori, S., van Zijl, P.C., Valavanis, A., Kollias, S., Boesiger, P., 2004. SENSE-DTI at 3 T. *Magn. Reson. Med.* 51, 230–236.
- Jones, D.K., Basser, P.J., 2004. “Squashing peanuts and smashing pumpkins”: how noise distorts diffusion-weighted MR data. *Magn. Reson. Med.* 52, 979–993.
- Jones, D.K., Horsfield, M.A., Simmons, A., 1999. Optimal strategies for measuring diffusion in anisotropic systems by magnetic resonance imaging. *Magn. Reson. Med.* 42, 515–525.
- Kim, J.A., Koyama, R., Yamada, R.X., Yamada, M.K., Nishiyama, N., Matsuki, N., Ikegaya, Y., 2004. Environmental control of the survival and differentiation of dentate granule neurons. *Cereb. Cortex* 14, 1358–1364.
- Kimiwada, T., Juhasz, C., Makki, M., Muzik, O., Chugani, D.C., Asano, E., Chugani, H.T., 2006. Hippocampal and thalamic diffusion abnormalities in children with temporal lobe epilepsy. *Epilepsia* 47, 167–175.
- Kurian, M., Spinelli, L., Delavelle, J., Willi, J.P., Velazquez, M., Chaves, V., Habre, W., Meagher-Villemure, K., Roulet, E., Villeneuve, J.G., Seeck, M., 2007. Multimodality imaging for focus localization in pediatric pharmacoresistant epilepsy. *Epileptic Disord.* 9, 20–31.
- Le Bihan, D., Poupon, C., Amadon, A., Lethimonnier, F., 2006. Artifacts and pitfalls in diffusion MRI. *J. Magn. Reson. Imaging* 24, 478–488.
- Lin, C.P., Tseng, W.Y., Weng, J.C., Wedeen, V.J., Chen, J.H., 2003a. Reduced encoding of diffusion spectrum imaging with cross-term correction. *Proceedings of the 1st IEEE EMBS Conference on Neural Engineering, Capri Island, Italy*, pp. 561–563.
- Lin, C.P., Wedeen, V.J., Chen, J.H., Yao, C., Tseng, W.Y., 2003b. Validation of diffusion spectrum magnetic resonance imaging with manganese-enhanced rat optic tracts and ex vivo phantoms. *NeuroImage* 19, 482–495.
- Liu, Z., Yang, Y., Silveira, D.C., Sarkisian, M.R., Tandon, P., Huang, L.T., Stafstrom, C.E., Holmes, G.L., 1999. Consequences of recurrent seizures during early brain development. *Neuroscience* 92, 1443–1454.
- Mello, L.E., Cavalheiro, E.A., Tan, A.M., Kupfer, W.R., Pretorius, J.K., Babb, T.L., Finch, D.M., 1993. Circuit mechanisms of seizures in the pilocarpine model of chronic epilepsy: cell loss and mossy fiber sprouting. *Epilepsia* 34, 985–995.
- Mori, S., van Zijl, P.C., 1998. A motion correction scheme by twin-echo navigation for diffusion-weighted magnetic resonance imaging with multiple RF echo acquisition. *Magn. Reson. Med.* 40, 511–516.
- Nadler, J.V., 2003. The recurrent mossy fiber pathway of the epileptic brain. *Neurochem. Res.* 28, 1649–1658.
- Nairismagi, J., Grohn, O.H., Kettunen, M.I., Nissinen, J., Kauppinen, R.A., Pitkanen, A., 2004. Progression of brain damage after status epilepticus

- and its association with epileptogenesis: a quantitative MRI study in a rat model of temporal lobe epilepsy. *Epilepsia* 45, 1024–1034.
- Nairismagi, J., Pitkanen, A., Narkilahti, S., Huttunen, J., Kauppinen, R.A., Grohn, O.H., 2006. Manganese-enhanced magnetic resonance imaging of mossy fiber plasticity in vivo. *NeuroImage* 30, 130–135.
- Obenaus, A., Jacobs, R.E., 2007. Magnetic resonance imaging of functional anatomy: use for small animal epilepsy models. *Epilepsia* 48 (Suppl. 4), 11–17.
- Paxinos, G., Watson, C., 1996. *The Rat Brain in Stereotaxic Coordinates*. Academic Press.
- Racine, R.J., 1972. Modification of seizure activity by electrical stimulation. II. Motor seizure. *Electroencephalogr. Clin. Neurophysiol.* 32, 281–294.
- Reese, T.G., Heid, O., Weisskoff, R.M., Wedeen, V.J., 2003. Reduction of eddy-current-induced distortion in diffusion MRI using a twice-refocused spin echo. *Magn. Reson. Med.* 49, 177–182.
- Reese, T.G., Benner, T., Wang, R., Feinberg, D.A., Wedeen, V.J., 2006. Halving imaging time of whole brain diffusion spectrum imaging (DSI) by using simultaneous echo refocusing (SER) EPI. *Proceedings of the 14th Meeting of the International Society for Magnetic Resonance in Medicine, Seattle, USA*, p. 1044.
- Rugg-Gunn, F.J., Eriksson, S.H., Symms, M.R., Barker, G.J., Duncan, J.S., 2001. Diffusion tensor imaging of cryptogenic and acquired partial epilepsies. *Brain* 124, 627–636.
- Salmenpera, T.M., Simister, R.J., Bartlett, P., Symms, M.R., Boulby, P.A., Free, S.L., Barker, G.J., Duncan, J.S., 2006. High-resolution diffusion tensor imaging of the hippocampus in temporal lobe epilepsy. *Epilepsy Res.* 71, 102–106.
- Scharfman, H.E., 2007. The CA3 “backprojection” to the dentate gyrus. *Prog. Brain Res.* 163, 627–637.
- Scharfman, H.E., Goodman, J.H., Sollas, A.L., 2000. Granule-like neurons at the hilar/CA3 border after status epilepticus and their synchrony with area CA3 pyramidal cells: functional implications of seizure-induced neurogenesis. *J. Neurosci.* 20, 6144–6158.
- Scharfman, H.E., Sollas, A.L., Smith, K.L., Jackson, M.B., Goodman, J.H., 2002. Structural and functional asymmetry in the normal and epileptic rat dentate gyrus. *J. Comp. Neurol.* 454, 424–439.
- Shepherd, T.M., Ozarslan, E., King, M.A., Mareci, T.H., Blackband, S.J., 2006. Structural insights from high-resolution diffusion tensor imaging and tractography of the isolated rat hippocampus. *NeuroImage* 32, 1499–1509.
- Shepherd, T.M., Wirth III, E.D., Thelwall, P.E., Chen, H.X., Roper, S.N., Blackband, S.J., 2003. Water diffusion measurements in perfused human hippocampal slices undergoing tonic changes. *Magn. Reson. Med.* 49, 856–863.
- Siddiqui, A.H., Joseph, S.A., 2005. CA3 axonal sprouting in kainate-induced chronic epilepsy. *Brain Res.* 1066, 129–146.
- Stringer, J.L., Williamson, J.M., Lothman, E.W., 1989. Induction of paroxysmal discharges in the dentate gyrus: frequency dependence and relationship to afterdischarge production. *J. Neurophysiol.* 62, 126–135.
- Sutula, T., 2002. Seizure-induced axonal sprouting: assessing connections between injury, local circuits, and epileptogenesis. *Epilepsy Curr.* 2, 86–91.
- Sutula, T., Cascino, G., Cavazos, J., Parada, I., Ramirez, L., 1989. Mossy fiber synaptic reorganization in the epileptic human temporal lobe. *Ann. Neurol.* 26, 321–330.
- Thivard, L., Lehericy, S., Krainik, A., Adam, C., Dormont, D., Chiras, J., Baulac, M., Dupont, S., 2005. Diffusion tensor imaging in medial temporal lobe epilepsy with hippocampal sclerosis. *NeuroImage* 28, 682–690.
- Tseng, W.Y., Lin, C.P., Chen, J.H., Wedeen, V.J., 2002. Diffusion spectrum imaging of complex cortical cytoarchitecture in adult rats. *Proceedings of the 10th Meeting of the International Society for Magnetic Resonance in Medicine, Hawaii, USA*, p. 441.
- van Eijsden, P., Notenboom, R.G., Wu, O., de Graan, P.N., van Nieuwenhuizen, O., Nicolay, K., Braun, K.P., 2004. In vivo 1H magnetic resonance spectroscopy, T2-weighted and diffusion-weighted MRI during lithium-pilocarpine-induced status epilepticus in the rat. *Brain Res.* 1030, 11–18.
- Wall, C.J., Kendall, E.J., Obenaus, A., 2000. Rapid alterations in diffusion-weighted images with anatomic correlates in a rodent model of status epilepticus. *AJNR Am. J. Neuroradiol.* 21, 1841–1852.
- Wedeen, V.J., Hagmann, P., Tseng, W.Y., Reese, T.G., Weisskoff, R.M., 2005. Mapping complex tissue architecture with diffusion spectrum magnetic resonance imaging. *Magn. Reson. Med.* 54, 1377–1386.
- Weih, K.S., Driesel, W., von Mengershausen, M., Norris, D.G., 2004. Online motion correction for diffusion-weighted segmented-EPI and FLASH imaging. *Magma* 16, 277–283.
- Williams, P.A., Wuarin, J.P., Dou, P., Ferraro, D.J., Dudek, F.E., 2002. Reassessment of the effects of cycloheximide on mossy fiber sprouting and epileptogenesis in the pilocarpine model of temporal lobe epilepsy. *J. Neurophysiol.* 88, 2075–2087.